A Journal of the Gesellschaft Deutscher Chemiker

Angewandte International Edition GDCh Chemie

www.angewandte.org

## Accepted Article

**Title:** A Homoleptic Alkynyl-Ligated [Au13Ag16L24]3- Cluster as a Catalytically Active Eight-Electron Superatom

**Authors:** Gao Li, Hannu Hakkinen, Zhaoxian Qin, Sachil Sharma, Chong-qing Wan, Wen-wu Xu, and Sami Malola



**To be cited as:** *Angew. Chem. Int. Ed.* 10.1002/anie.202011780

**Link to VoR:** https://doi.org/10.1002/anie.202011780

WILEY-VCH

10.1002/anie.202011780

WILEY-VCH

# A Homoleptic Alkynyl-Ligated $[Au_{13}Ag_{16}L_{24}]^{3-}$ Cluster as a Catalytically Active Eight-Electron Superatom

Zhaoxian Qin,[a,b] Sachil Sharma,[b] Chong-qing Wan,[a]* Sami Malola,[c] Wen-wu Xu,[d] Hannu Häkkinen[c]*, and Gao Li[b,e]*

**Abstract:** A brand new alkynylated cluster $[Au_{13}Ag_{16}(C_{10}H_6NO)_{24}]^{3-}$ is prepared by $NaBH_4$ mediated reduction method. The AuAg clusters are confirmed by various sophisticated characterization techniques. It manifested the unique metal framework of "$Au_{center}@Ag_{12}@Au_{12}Ag_4$" is protected by 24 atypical alkyne ligands L (L = $C_{10}H_6NO$). The ligands were found to construct a unique type of motif L-(Ag)-Au-(Ag)-L at the cluster interface, where, the alkyne (C≡C) group of each L was linked by sharing an Au atom through the $\sigma$ bonds and each C≡C group was discretely connected to chemically different Ag atom ($Ag_{icosahedral}$/$Ag_{cap}$) through $\pi$ bonds. The electronic and optical properties of $[Au_{13}Ag_{16}L_{24}]^{3-}$ were studied in detail. DFT characterized the cluster as a clear 8-electron superatom, and peaks in the optical absorption spectrum were successfully interpreted in terms of the P and D superatom states. The supported $Au_{13}Ag_{16}L_{24}/CeO_2$ catalyst exhibited high catalytic activity and selectivity towards the $A^3$-coupling reaction involving benzaldehyde, diethylamine and phenylacetylene.

Recently, the structure-property relationships of the ligand-protected metal clusters[1] have attracted tremendous interest owing to their precise crystal structures and size specific molecule-like properties, such as HOMO-LUMO gaps,[1a] chirality,[2] photoluminescence,[3] magnetism,[4] redox behaviour,[5] and catalytic activity,[6] not observed in bulk metals. These clusters are usually protected by complex mono-layers of organic molecules including phosphine, chalcogenolate (-SR, -SeR, and -TeR) and alkyne ligands.[7] Due to the weak M-P (M =Au/Ag) bonds on the cluster surface, phosphine protected metal clusters have poor stability, which hindered their applications.[8] And, the high strength of M-S bond led to the extensive study of thiolate-protected clusters $M_n(SR)_m$, which has been exploited in nanocatalysis, imaging, nanomedicine etc.[1a,1b,9]

[a] Z. Qin, Prof. C.-q. Wan
Beijing Key Laboratory for Optical Materials and Photonic Devices, Department of Chemistry, Capital Normal University, Beijing 100048, China E-mail: wancq@cnu.edu.cn
[b] Z. Qin, Dr. S. Sharma & Prof. G. Li
State Key Laboratory of Catalysis, Dalian Institute of Chemical Physics, Chinese Academy of Sciences, Dalian 116023, P. R. China
E-mail: gaoli@dicp.ac.cn
[c] Dr. S. Malola, Prof. H. Häkkinen
Departments of Physics and Chemistry, Nanoscience Center, University of Jyväskylä, FI - 40014 Jyväskylä, FINLAND
Email: hannu.j.hakkinen@jyu.fi
[d] Prof. W. W. Xu
Department of Physics, School of Physical Science and Technology, Ningbo University, Ningbo, 315211, China.
[e] Prof. G. Li
University of Chinese Academy of Sciences, Beijing 100049, China
CCDC: 2009603
Supporting information and the ORCID identification number(s) for the author(s) of this article can be found under:

In the last few years, the emerging structurally precise alkyne protected metal clusters[10] drew a lot of attention, which appeared to be a new class of nanoclusters with many diffrences in structures and physichemical properties from above mentioned chalcogenolatecounterparts. The alkyne groups can coordinate with surface of metal clusters via $\sigma$ and $\pi$ interactions, which is distinct to thiolate-metal staples -S(R)[-Au-S(R)-]$_x$ in $M_n(SR)_m$[11]. The five types of complex coordination modes of alkynes on the surface of metal clusters are described in literatures, which can tune their electronic structure through $\pi$-conjugation.[10a,12] Recently, Wang et al reported a series of structurally precise alkynylate metal clusters including[10a]: (a) mixed alkyne and phosphine protected monometallic clusters[13], namely $Au_{19}PA_9(hdppa)_3$ (PA: phenylacetylene, hdppa: diphenylphosphinoamine), $[Au_{23}PA_9(PPh_3)_6]^{2+}$, $[Au_{40}PA_{20}(dppm)_4]^{4+}$ (dppm: bis(diphenylphosphinomethane), $[Au_{38}PA_{20}(PPh_3)_4]^{2+}$, $[Au_{24}PA_{14}(PPh_3)]^{2+}$, $[Ag_{19}PA_{14}(dppm)_3]^{3+}$ and $[Ag_{25}(C{\equiv}CC_6H_4OCH_3)_{20}(dppp)_3]^{3+}$ (dppp: bis(diphenylphosphino)-pentane), and (b) the homoleptic alkyne protected gold clusters,[14] such as $[Au_{25}(C{\equiv}CAr)_{18}]^-$, $Au_{36}PA_{24}$, $Au_{44}PA_{28}$, $Au_{144}(C{\equiv}CC_6H_4F)_{60}$, $Au_{22}(^tBuC{\equiv}C)_{18}$, $[Au_{23}(C{\equiv}C^tBu)_{15}]$, $Au_{42}(C{\equiv}CC_6H_4CF_3)_{22}$, and $Au_{50}(C{\equiv}CC_6H_4F)_{26}$. In addition, the crystal structures of Au-Ag bimetallic clusters with composition,[15] e.g. $Au_{34}Ag_{28}PA_{34}$, $[Au_{80}Ag_{30}PA_{42}Cl_9]^+$, $[Au_4Ag_{23}(C{\equiv}C^tBu)_{10}(dppf)_4Cl_7]^{2+}$, $Au_{57}Ag_{53}PA_{40}Br_{12}$, $Au_5Ag_{24}(C{\equiv}CC_6H_4{}^tBu)_{16}(dppf)_4Cl_4]^{3+}$ and $Au_{24}Ag_{20}PA_{20}(SPy)_4Cl_2$ (SPy: pyridylthiolate), were also reported. The most of the above listed alkynylated clusters, such as $Au_{19}$, $Au_{23}$, $Au_{25}$ $Au_{144}$, $Au_{57}Ag_{53}$, and $Au_{80}Ag_{30}$ were found to be very stable over a period of month or more under the ambient conditions. However, still some issues are there to be addressed: (1) the aforementioned $Au_{34}Ag_{28}$[15a] is the only-example of homoleptic alkynylated Au and Ag bimetal cluster with precise crystal structure and (2) so far, the phenyl acetylene i.e. the simplest known aromatic alkyne has been regularly used to protect the metal clusters. Furthermore, once the phenyl group is replaced or a new functional group is added to phenyl group, its effect on coordination model, structure and properties remained unclear. Hence, in order to expand the library of homoleptic alkynylated Au and Ag bimetal cluster for gaining deep insight, it becomes essential to synthesize and determine the precise structure of the novel bimetal nanoclusters protected by atypical homoleptic alkyne ligands.

Herein, we report the synthesis, crystal structure, and properties of a new homoleptic alkynyl protected 29-metal atoms bimetal cluster with the composition of $Au_{13}Ag_{16}(C_{10}H_6NO)_{24}$. The single-crystal X-ray structure exhibits nonhollow $Au@Ag_{12}$ icosahedron metal core (kernel), exterior of 4 $AgAu_3$ capping units attached to icosahedral Ag atoms through metal-metal bonds, and overall the $Au@Ag_{12}@Au_{12}Ag_4$ metal framework is protected by 24 ligands coordinating with Au and Ag atoms via $\sigma$ and $\pi$ bonds, respectively. The unique type of L-(Ag)-

10.1002/anie.202011780



Au-(Ag)-L motif distinct to staple motif of $M_n(SR)_m$ was formed at the metal-ligand interface. We further investigated the catalytic activity of $Au_{13}Ag_{16}L_{24}$ towards $A^3$-coupling reaction after loading them on $CeO_2$ or $TiO_2$ support.

The bimetallic $Au_{13}Ag_{16}L_{24}$ (ionized 2-(prop-2-ynyloxy)benzonitrile abbreviated as L, hereafter) clusters was prepared by direct $NaBH_4$ reduction (Figures S1-S4 in SI). Firstly, Au-L and Ag-L were synthesized in our lab. Subsequently, into the mixture of Au-L and Ag-L solutions, a freshly prepared solution of $NaBH_4$ was added dropwise under vigorous stirring with the immediate color change from gray to black. The reaction solution was stirred in the dark for ~ 72 h until the molecular-like absorption bands appeared at 350 nm, 443 nm and 610 nm in the UV-Vis spectrum (Figure 5a, vide infra). Further, in order to confirm the composition and understand the coordination modes of alkyne ligand (L) at the metal-ligand interface by single crystal X-ray diffraction (See S5 in SI), the crystals were grown by vapor diffusion of ether into the concentrated dichloromethane solution of clusters at ~10 ºC over one month in dark.

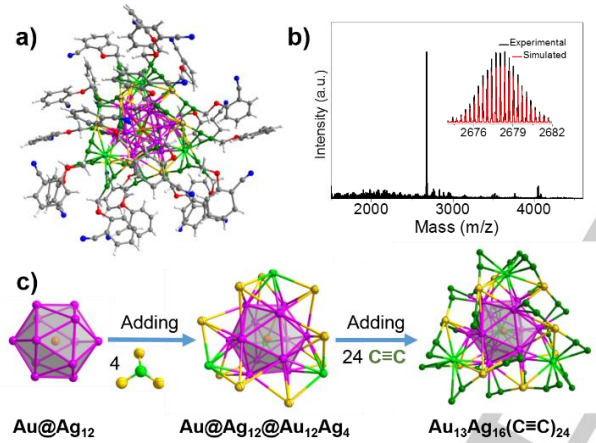


**Figure 1**. (a) Total structure of the $Au_{13}Ag_{16}L_{24}$ clusters. (b) Negative-mode ESI mass spectrum of the $Au_{13}Ag_{16}L_{24}$ cluster (inset: the experimental and simulated isotopic distribution patterns). (c) $Au@Ag_{12}@Au_{12}Ag_4$ metal framework protected by alkyne groups from 24 ligands, with only C≡C groups (highlighted in green) of L shown here for clarity. Color codes: Au, yellow, orange; Ag, purple and bright green; C, grey and green; N, blue; O, red.

The total structure of synthesized cluster determined by the single-crystal X-ray diffraction is shown in Figure 1a. The cluster was crystallized in a triclinic P-1 space group and the composition was determined to be $Au_{13}Ag_{16}(C_{10}H_6NO)_{24}$. Further, the precise composition was also verified using ESI mass spectrometry; no additive was added during the ESI-MS experiments. Only one intense peak at m/z 2678.03 Da in the range of m/z 1500 to 4500 Da is displayed in the negative ion ESI mass spectrum, as shown in Figure 1b and the spacing between the experimental isotopic peaks is found to be ~0.333 Da, indicating that the cluster ion has a charge of minus three. Hence, the cluster mass is evaluated to be 8034.09 Da (i.e. 2678.03 Da × 3), which corresponds to exact composition of $Au_{13}Ag_{16}C_{240}H_{144}N_{24}O_{24}$ (theoretical mass ~8034.3 Da), as revealed in the SC-XRD results. The molecular formula of the prepared bimetallic clusters is identified as $[Au_{13}Ag_{16}L_{24}]^{3-}$; the cations should be $Na^+$, confirmed by the XPS results.

As depicted in Figure 1c, the $Au_{13}Ag_{16}L_{24}$ clusters exhibit a non-hollow icosahedron metal core $Au@Ag_{12}$ with Au atom at its center and 12 Ag atoms on icosahedron surface sites. The similar type of $Au@Ag_{12}$ icosahedron metal cores have also been earlier reported in the structures of $[AuAg_{24}(SPhMe_2)_{18}]^-$ and $[AuAg_{20}\{Se_2P(OEt)_2\}_{12}]^+$ clusters.[16] The radial $Au_{center}$-$Ag_{icosa}$ and peripheral $Ag_{icosa}$-$Ag_{icosa}$ bond lengths in our study were calculated to be in the range of 2.786-2.853 Å (average 2.820 Å) and 2.907-3.044 Å (average 2.965 Å), respectively, which are slightly longer than the radial Au-Ag and peripheral Ag-Ag bond lengths in $[Ag_{24}Au(SPhMe_2)_{18}]^-$ (radial Au-Ag = 2.744-2.792 Å, peripheral Ag-Ag = 2.861-2.978 Å),[16a] $[AuAg_{20}\{Se_2P(OEt)_2\}_{12}]^+$ (average Au-Ag = 2.777 Å)[16b] and $[Ag_{29}(BDT)_{12}(TPP)_4]^{3-}$ (average radial Ag-Ag = 2.77 Å and average peripheral Ag-Ag = 2.92 Å).[17] In the exterior, $Au@Ag_{12}$ core is capped by four $AgAu_3$ units through $Au_{cap}$-$Ag_{icosa}$ bonds in range of 2.891-3.214 Å (average 3.032 Å) and $Ag_{cap}$-$Ag_{icosa}$ bonds in the range 2.868-3.004 Å (average 2.941 Å) forming the complete 29 metal atom framework with the composition of $Au@Ag_{12}@Au_{12}Ag_4$, which is diffrent from those observed in reported $Ag_{29}$[17] and $AuAg_{28}$ clusters[18]. The $Au_{cap}$-$Ag_{cap}$ bond lengths in the all four $AgAu_3$ units were found to be in the range of 2.926-3.126 Å (average = 3.029 Å).

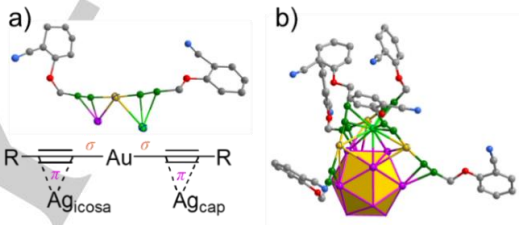


**Figure 2.** The coordination mode of alkynyl ligand L at the interface of $Au_{13}Ag_{16}L_{24}$. Color code: Au, yellow; Ag, purple and bright green; C, grey and green; N, blue; O, red.

The metal framework of $Au_{13}Ag_{16}$ comprised of an $Au@Ag_{12}$ core and an exterior of four $AgAu_3$ capping units is protected by 24 alkynyl ligands in unique coordination mode. Figure 2a shows each alkynylate L adopts a $\mu_2$-$\eta^1$ (Au), $\eta^2$ (Ag) coordination mode, where alkyne C≡C group coordinate with one Au atom via $\sigma$ bond (average Au-C: ~2.08 Å) and one Ag atom through a $\pi$ bond (average Ag-C: ~2.52 Å). More importantly here, the C≡C groups of pair of alkynyl ligands (L) is linked by sharing an Au atom through $\sigma$ bonds and each C≡C group are connected separately with chemically different Ag atom (i.e. $Ag_{icosa}$/$Ag_{cap}$) through $\pi$ bonds forming 12 linear "L-($Ag_{cap}$)-Au-($Ag_{icosa}$)-L" type of motifs, exactly similar to the coordination mode shown in Figure 2b. Such similar type of linear $\pi$ motifs on Au surface were theoretically calculated to be energetically more stable,[19] which is also experimentally observed in the crystal structures of $Au_{34}Ag_{28}PA_{34}$,[15a] $[Au_{80}Ag_{30}PA_{42}Cl_9]Cl$,[15c] and $Au_{24}Ag_{20}PA_{20}$(2-py-S)$_4Cl_2$[15f]. The subtle distinction in our study is that, $\pi$ bonds are rather formed on the Ag atoms at the interface of alkynylated $Au_{13}Ag_{16}$. Furthermore, three pairs of linear "L-($Ag_{cap}$)-Au-($Ag_{icosa}$)-L" construct an $AgAu_3L_6$ unit by sharing an $Ag_{cap}$ atom and these $AgAu_3L_6$ units were found connected to the surface of $Au@Ag_{12}$ core through Au-Ag metal bonds as illustrated in Figure 2b. Thus, the overall structure of $Au_{13}Ag_{16}L_{24}$ is dictated by atypical alkynyl ligand L and was also found

10.1002/anie.202011780

WILEY-VCH

to be a cubic cluster rather than the tetravalent ones observed in other 29-metal clusters e.g. thiolate protected $Ag_{29}$[17] and $AuAg_{28}$[18].

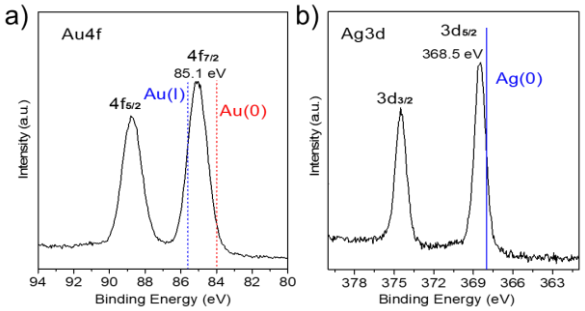


**Figure 3**. (a) Au 4f XPS spectrum and (b) Ag 3d XPS spectrum of $Au_{13}Ag_{16}L_{24}$ clusters.

The $Au_{13}Ag_{16}L_{24}$ clusters were further characterized by various spectroscopic techniques such as XPS and UV-Vis. The wide scan XPS survey spectrum of $Au_{13}Ag_{16}$ (Figure S5 in SI) suggested the presence of all expected six elements including Au, Ag, C, N, O and Na. No other impurity was detected by XPS. In Au 4f XPS spectrum shown in Figure 3a, the Au $4f_{7/2}$ peak centered at 85.1 eV is shifted to high binding energy with respect to $Au^0$ (83.9 eV)[20], which is attributed to presence of both $Au^0$ and $Au^I$ in the cluster. Here $Au^0$ corresponds to only central Au atom of $Au@Ag_{12}$ core, while $Au^1$ corresponds to 12 Au atoms belonging to 4 $AgAu_3$ capping units in the exterior shell. Similarly, in Ag 3d spectrum (Figure 3b), the Ag $3d_{5/2}$ peak at 368.5 eV was found slightly on the higher binding energy side compared to standard $Ag^0$ (368.0 eV)[20]. This suggests the existence of Ag atoms mostly in slightly negative charged state in the $Au_{13}Ag_{16}L_{24}$ cluster. Here, the shifts detected in the XPS spectra for Au and Ag is probably caused by formation of L-(Ag)-Au-(Ag)-L motif on metal surface in $Au_{13}Ag_{16}L_{24}$.

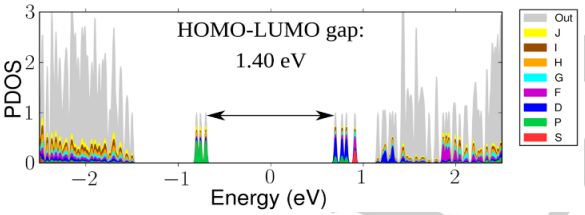


**Figure 4**. The electronic density of states of the $[Au_{13}Ag_{16}L_{24}]^{3-}$ cluster as projected to spherical harmonics centered at the metal core. The occupied/unoccupied states are shown with negative/positive energies, respectively, with the HOMO-LUMO energy gap.

The electronic structure and optical absorption of $[Au_{13}Ag_{16}L_{24}]^{3-}$ were investigated by using the implementation of DFT in a real-space code GPAW[21], see details in SI. The electronic density of states at the ground state shows a rather large energy gap (1.4 eV) between the highest occupied (HOMO) and lowest unoccupied (LUMO) molecular orbitals (Figure 4). Projection of the frontier orbitals to spherical harmonics reveals a set of three orbitals from HOMO-2 to HOMO having a clear P symmetry while the LUMO orbital has a D symmetry. This corresponds well to the expectation for 8-electron closed-shell system from the so-called superatom model.[22] $Au_{13}Ag_{16}L_{24}$ cluster is found to be very stable over a month under ambient conditions (Figure S6 in SI), which may be due to the closed shell (8 $e^-$) electronic system of the clusters.

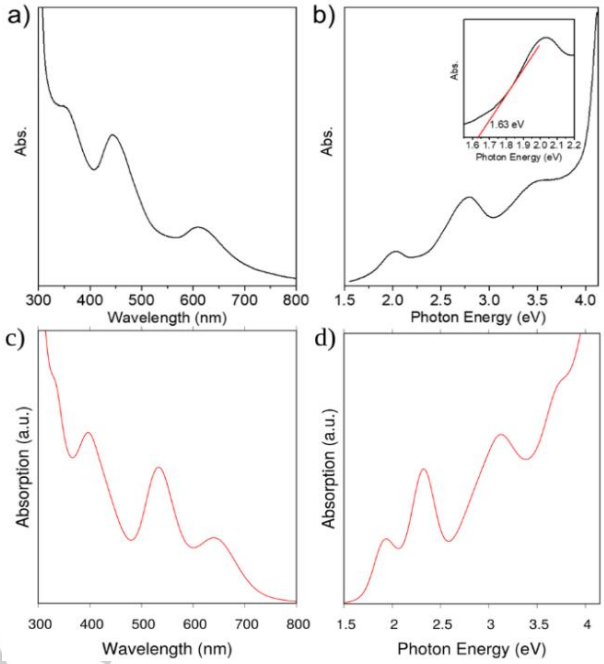


**Figure 5**. The experimental (a), (b) and computed (c), (d) UV-Vis spectra of $[Au_{13}Ag_{16}L_{24}]^{3-}$ both in wavelength and energy scales. The inset in (b) shows extrapolation of the experimental data to estimate the value for the optical gap (1.63 eV).

And, the high stability also may be plausibly attributed to formation of energetically favorable L-(Ag)-Au-(Ag)-L motif at the metal-ligand interface (vide supra) in $Au_{13}Ag_{16}L_{24}$. Furthermore, it is interesting to note that several other empty states above the LUMO have also well-behaving symmetries (D and S) as expected from the superatom model. Splitting of the empty states in two “bands” will be reflected in the analysis of the optical absorption spectrum discussed next.

As shown in Figures 5a, b, $Au_{13}Ag_{16}L_{24}$ exhibits three main molecular absorption bands at 350 nm, 443 nm, and 610 nm in the UV-Vis region, which is quite distinct from other 29 metal atoms clusters with compositions of $Ag_{29}(BDT)_{12}(TPP)_4$,[17] $Au_{29}(SR)_{20}$[23] and $Ag_{28}Au(BDT)_{12}(TPP)_4$[18] reported earlier in the literature. The estimated optical energy gap ≈1.63 eV (inset of Figure 5b) was also found to be lower than the aforementioned 29 metal atoms thiolated counterparts and compares rather well with the aforementioned theoretical HOMO-LUMO gap of 1.4 eV.

The computed absorption spectrum of $[Au_{13}Ag_{16}L_{24}]^{3-}$ is shown in Figures 5c, d. It also shows three distinct peaks at 396 nm, 533 nm, and 641 nm, in excellent agreement with the experimental data, although all peaks are somewhat red-shifted as compared to experiment, which is rather typical for the used PBE functional. The character of the electron-hole transitions contributing to these peaks was analyzed via the so-called Dipole Transition Contribution Maps (DTCM) shown in Figure 6. This analysis gives a very clear interpretation of the peaks as follows. The lowest-energy peak at 641 nm has essentially two components: (i) dipole increasing P → D and P → S transitions from {HOMO-2⋯HOMO} states to four unoccupied

10.1002/anie.202011780



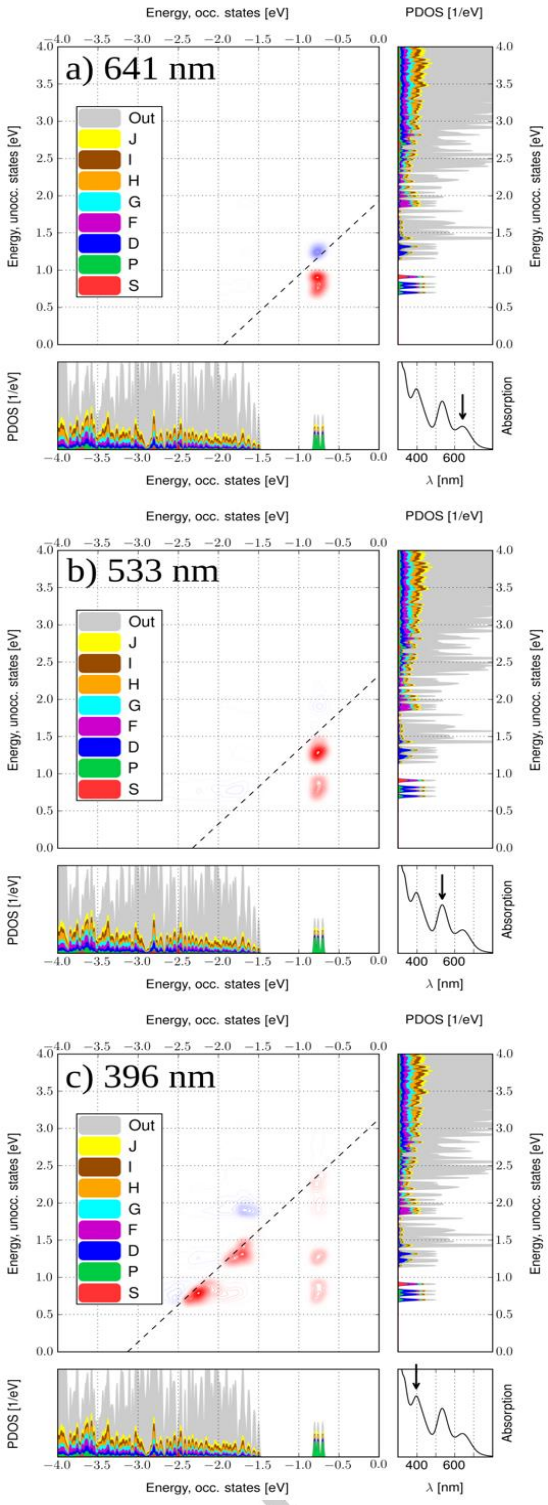


**Figure 6.** Dipole transition contribution maps (DTCM) for the three peaks at 641 nm, 533 nm, and 396 nm in the computed absorption spectrum of $[Au_{13}Ag_{16}L_{24}]^{3-}$ as marked in bottom-right panels of each sub-figure. Each map shows contributions to the given absorption peak by transitions from occupied single electron states to unoccupied states as shown at horizontal bottom and vertical right panels, respectively. Red/blue areas in the maps denote contributions that increase/decrease the total dipole moment of the absorption. The dashed lines in the maps denote positions where the created electron-hole pairs have the energy that is equal to the analyzed absorption peak energy.

{LUMO···LUMO+3} states and (ii) dipole screening P → D transitions from {HOMO-2···HOMO} to the higher energy unoccupied states with D character. The second peak at 533 nm has all the same contributions as the first peak, but now all transitions are strengthening the total dipole. Finally, the third peak at 396 nm has strong dipole-increasing transitions originating from the occupied states around -1.7 eV and -2.3 eV to the aforementioned empty superatom D and S states. It is the compressed nature of the empty final states that makes the local absorption maximum at that area in the spectrum.

Recently, the metal clusters catalyzed three components coupling reaction (e.g. $A^3$-coupling) to synthesize propargylamines has drawn much attention.[24] One of unique feature of structurally precise metal clusters as catalysts is that they provide a platform to establish relationship between their structure and catalytic properties. Therefore, we loaded the $Au_{13}Ag_{16}$ clusters on oxides as the catalysts for the $A^3$-coupling. Briefly, the $Au_{13}Ag_{16}L_{24}$ clusters were dissolved in a dichloromethane solution followed by the soaking of oxide powder in the cluster solution under vigorous stirring in a sealed vial. Subsequently, the $Au_{13}Ag_{16}L_{24}/CeO_2$ catalyst was collected by centrifugation and dried at 100 °C in air (See more details in SI).

It is worth to mention here that the UV-Vis absorption spectrum of ligand protected metal cluster with molecular purity usually provides a reliable tool to distinguish them. Hence, we measured the UV-Vis spectra of $Au_{13}Ag_{16}L_{24}$ clusters in solution and after their loading on $CeO_2$. As shown in Figure S7, the two bands at 450 nm and 610 nm in solid state UV-Vis spectra of the fresh and spent $Au_{13}Ag_{16}L_{24}/CeO_2$ powders were in good agreement with the UV-Vis spectrum of $Au_{13}Ag_{16}$ in solution in the range of 378-800 nm. Futher, TEM also showed that metal particles on the $CeO_2$ support is ~1.5 nm, in good agreement with size of the free clusters. These results clearly suggests that the structure of the $Au_{13}Ag_{16}L_{24}$ cluster remained intact after supporting them on oxides. Then the oxide-supported $Au_{13}Ag_{16}L_{24}$ was utilized as a catalyst for the $A^3$-coupling reaction of benzaldehyde, phenylacetylene and diethylamine, and compared with the thiolate-protected $Au_{25}(SR)_{18}$ and $Au_{25-x}Ag_x(PPh_3)_{10}(SPh)_5Cl_2$ (where, $0 < x < 13$) nanoclusters.

The catalytic results are summarized in Table 1. Firstly, the bare $CeO_2$, $TiO_2$, and free $Au_{13}Ag_{16}L_{24}$ clusters were catalytically tested to study their performance towards the $A^3$-coupling reaction. The GC-MS results suggested the aldehyde conversion was only ~2% for $CeO_2$ and $TiO_2$, indicating very low catalytic activity of the bare oxides. And a low conversion of ~19% is observed in the free $Au_{13}Ag_{16}L_{24}$ catalyzed reaction. Then, the coupling reaction was performed under the same conditions using oxide-supported $Au_{13}Ag_{16}L_{24}$, $Au_{25}(SR)_{18}$, and $Au_{25-x}Ag_x(PPh_3)_{10}(SPh)_5Cl_2$ nanoclusters as catalyst. Interestingly, $Au_{13}Ag_{16}/CeO_2$ exhibited very good catalytic activity with a high conversion of 89%, which is similar with that over $Au_{25}(PPh_3)_{10}(C{\equiv}CPh)_5Cl_2$[24b] and much higher than those of oxide-supported $Au_{38}(SC_2H_4Ph)_{24}$,[24a] $Au_{25}(SC_2H_4Ph)_{18}$, and $Au_{25-x}Ag_x(PPh_3)_{10}(SPh)_5Cl_2$. A strong ligand effect is observed in the cluster-catalyzed $A^3$-coupling reaction.[25] It is worthwhile to mention here that even 0.5 wt% of loaded clusters improved the catalytic performance of $CeO_2$ significantly. In a separate experiment, $Au_{13}Ag_{16}/TiO_2$ catalyst was tested for the $A^3$-coupling reaction, a subtle low conversion about 75% was detected. The delicate difference is perhaps caused by the different nature of the cluster-

support interactions in these systems. Furthermore, we tested the recyclability of $Au_{13}Ag_{16}/CeO_2$ catalyst (Table 1, entries 10 and 11). A decrease on aldehyde conversion was observed at the higher recycle number, which is mainly due to the loss of the $Au_{13}Ag_{16}$ nanoclusters during the reactions (Figures S8 and S9).[24b]

**Table 1**. Catalytic performance of $Au_{13}Ag_{16}L_{24}$/oxide catalysts in the $A^3$-coupling reaction. Reaction conditions: benzaldehyde (1 mmol), phenylacetylene (1.3 mmol), diethylamine (1.2 mmol), $Au_{13}Ag_{16}L_{24}$/oxide (50 mg, ~ 0.5 wt% cluster loading), 5 mL MeCN, at 100 °C for 24 h.

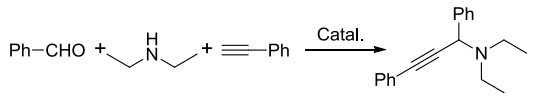


| entry | catalyst | conversion | selectivity |
|---|---|---|---|
| 1 | $CeO_2$ | 2% | 100% |
| 2 | $TiO_2$ | 2% | 100% |
| 3 | free $Au_{13}Ag_{16}L_{24}$ | 19% | 100% |
| 4 | $Au_{13}Ag_{16}/CeO_2$ | 89% | 100% |
| 5 | $Au_{13}Ag_{16}/TiO_2$ | 75% | 100% |
| 6 | $Au_{25-x}Ag_x/CeO_2$ | 13% | 100% |
| 7 | $Au_{38}(SR)_{24}/CeO_2$ | 26% | 100% |
| 8 | $Au_{25}(SR)_{24}/CeO_2$ | 16% | 100% |
| 9 | $Au_{25}PA_5/CeO_2$ | 91% | 100% |
| 10 [a] | $Au_{13}Ag_{16}/CeO_2$ | 80% | 100% |
| 11 [b] | $Au_{13}Ag_{16}/CeO_2$ | 75% | 100% |

**Note:** $Au_{13}Ag_{16}$, $Au_{25}PA_5$, and $Au_{25-x}Ag_x$ represent the $Au_{13}Ag_{16}(L)_{24}$, $Au_{25}(PPh_3)_{10}(C{\equiv}CPh)_{24}Cl_2$, and $Au_{25-x}Ag_x(PPh_3)_{10}(SPh)_5Cl_2$, respectively. [a] 2nd cycle. [b] 3rd cycle.

In summary, we have synthesized a novel homoleptic alkyne protected bimetallic cluster with the composition of $Au_{13}Ag_{16}L_{24}$, where $L=C_{10}H_6NO$, for the first time. Single-crystal X-ray structural analysis reveals that it is composed of non-hollow $Au@Ag_{12}$ icosahedron, which is capped by 4 $AgAu_3L_6$ exterior units through metal-metal bonds. The overall metal frame work "$Au@Ag_{12}@Ag_4Au_{12}$" is protected by 24 ligands in unique fashion. Here, a pair of ligands (L) constructs a special type of motif "L-($Ag_{cap}$)-$Au_{cap}$-($Ag_{icosa}$)-L" at the metal-ligand interface. In this motif, the alkyne group (C≡C) of each ligand L is linked by sharing an $Au_{cap}$ atom. However, each C≡C group of the motif is individually connected with chemically different Ag atom (icosahedral or capping Ag) through $\pi$ bonds. DFT characterized the cluster as a clear 8-electron superatom, and peaks in the optical absorption spectrum were successfully interpreted in terms of the P and D superatom states. Interestingly, the $Au_{13}Ag_{16}L_{24}$ clusters displayed high stability under ambient conditions and the high catalytic activity in the $A^3$-coupling reactions.

## Acknowledgements

We thank the financial support by Liaoning Natural Science Foundation of China (2020-MS-024), Liaoning Revitalization Talents Program (XLYC1807121), NSF of Beijing Municipality (2172014) and Capacity Building for Sci-Tech Innovation-Fundamental Scientific Research Funds. The theoretical work at University of Jyväskylä was supported by the Academy of Finland (grants 292352 and 319208). The computations were made at the Finnish supercomputing center CSC and at the Barcelona Supercomputing Center as part of a PRACE project.

## Conflict of interest

The authors declare no conflict of interests

**Keywords:** AuAg alloy cluster, alkynyl, $A^3$-coupling, density functional theory, eight-electron superatom

[1] a) R. Jin, C. Zeng, M. Zhou, Y. Chen, *Chem. Rev.* **2016**, 116, 10346-10413; I. Chakraborty, T. Pradeep, *Chem. Rev.* **2017**, 117, 8208-8271; c) B. Bhattarai, Y. Zaker, A. Atnagulov, B. Yoon, U. Landman, T. P. Bigioni, *Acc. Chem. Res.* **2018**, 51, 3104-3113; d) X. Liu, D. Astruc, *Coord. Chem. Rev.* **2018**, 359, 112-126.

[2] B. Nieto-Ortega, T. Bürgi, *Acc. Chem. Res.* **2018**, 51, 2811-2819.

[3] X. Kang, M. Zhu, *Chem. Soc. Rev.* **2019**, 48, 2422-2457.

[4] M. Agrachev, M. Ruzzi, A. Venzo, F. Maran, *Acc. Chem. Res.* **2019**, 52, 44-52.

[5] K. Kwak, D. Lee, *Acc. Chem. Res.* **2019**, 52, 12-22.

[6] a) G. Li, R. Jin, *Acc. Chem. Res.* **2013**, 46, 1749-1758; b) T. Higaki, Y. Li, S. Zhao, Q. Li, S. Li, X. S. Du, S. Yang, J. Chai, R. Jin, *Angew. Chem. Int. Ed.* **2019**, 58, 8291-8302.

[7] a) P. D. Jadzinsky, G. Calero, C. J. Ackerson, D. A. Bushnell, R. D. Kornberg, *Science*, **2007**, 318, 430-433; b) X. Kang, M. Zhu, *Small*, **2019**, 15, 1902703; c) W. Kurashige, S. Yamazoe, M. Yamaguchi, K. Nishido, K. Nobusada, T. Tusukuda, Y. Negishi, *J. Phys. Chem. Lett.* **2014**, 5, 2072-2076.

[8] W. Kurashige, Y. Negishi, *J. Cluster Sci.* **2012**, 23, 365-374.

[9] Y. Du, H. Sheng, D. Astruc, M. Zhu, *Chem. Rev.* **2020**, 120, 526-622.

[10] a) F. Mirkhalaf; J. Paprotny; D. J. Schiffrin. *J. Am. Chem. Soc.* **2006**,128, 7400-7401; b) P. Maity, H. Tsunoyama, M. Yamauchi, S. Xie, T. Tsukuda, *J. Am. Chem. Soc.* **2011**, *133*, 20123-20125.

[11] T. Tsukuda, H. Häkkinen, Protected Metal Clusters: From Fundamentals to Applications, Elsevier B.V., Amsterdam, The Netherlands, Vol 9 1st Edn, **2015**, pp. 9-38.

[12] Z. Lei, X. K. Wan, S. F. Yuan, J.-Q. Wang, Q. M. Wang, *Dalton Trans.* **2017**, 46, 3427-3434.

[13] a) T. Wang, W. H. Zhang, S. F.Yuan, Z. J. Guan, Q. M. Wang, *Chem. Commun.* **2018**, 54,10367-10370; b) X. K. Wan, Q. Tang, S. F. Yuan, D. E. Jiang, Q. M. Wang, *J. Am. Chem. Soc.* **2015**,137, 652-655; c) X. K. Wan, S. F. Yuan, Q. Tang, D. E. Jiang, Q. M. Wang, *Angew. Chem. Int. Ed.* **2015**, 54, 5977-5980; d) X. K. Wan, W. W. Xu, S. F. Yuan, Y. Gao, X. C. Zeng, Q. M. Wang, *Angew. Chem. Int. Ed.* **2015**, 54, 9683-9686; e) X. K. Wan, J. Q. Wang, Z. A. Nan, Q. M. Wang, *Sci. Adv.* **2017**, 3, e1701823; f) S. F. Yuan, P. Li, Q. Tang, X. K. Wan, Z. A. Nan, D. Jiang, Q. M. Wang, *Nanoscale* **2017**, 9, 11405-11409.

[14] a) J. J. Li, Z. J. Guan, Z. Lei, F. Hu, Q. M. Wang, *Angew. Chem. Int. Ed.* **2019**, 58, 1083-1087; b) X. K. Wan, Z. J. Guan, Q. M. Wang, *Angew. Chem. Int. Ed.* **2017**, 56, 11494-11497; c) Z. Lei, J. J. Li, X. K. Wan, W. H. Zhang, Q. M. Wang, *Angew. Chem. Int. Ed.* **2018**, 57, 8639-8643; d) X. S. Han, X. Luan, H. F. Su, J. J. Li, S. F. Yuan, Z. Lei, Y. Pei, Q. M. Wang, *Angew. Chem. Int. Ed.* **2020**, 59, 2309-2312; e) Z. J. Guan, F. Hu, J. J. Li, Z. R. Wen, Y. M. Lin, Q. M. Wang, *J. Am. Chem. Soc.* **2020**,142, 2995-3001; f) Z. J. Guan, F. Hu, J. J. Li, Z. R. Liu, Q. M. Wang, *Nanoscale* **2020**,12,13346-13350.

[15] a) Y. Wang, X. K. Wan, L. Ren, H. Su, G. Li, S. Malola, S. Lin, Z. Tang, H. Häkkinen, B. K. Teo, Q. M. Wang, N. Zheng, *J. Am. Chem. Soc.* **2016**, 138, 3278-3281; b) F. Hu, J. J. Li, Z. J. Guan, S. F. Yuan, Q. M. Wang, *Angew. Chem. Int. Ed.* **2020**, 59, 5312-5315; c) J. L. Zeng, Z. J. Guan, Y. Du, Z. A. Nan, Y. M. Lin, Q. M. Wang, *J. Am. Chem. Soc.* **2016**, 138, 7848-7851; d) Z. J. Guan, J. L. Zeng, S. F. Yuan, F. Hu, Y. M. Lin, Q. M.

Wang, *Angew. Chem. Int. Ed.* **2018**, 57, 5703-5707; e) Y. Du, Z. J. Guan, Z. R. Wen, Y. M. Lin, Q. M. Wang, *Chem. Eu. J.* **2018**, 24, 16029-16035; f) Y. Wang, H. Su, C. Xu, G. Li, L. Gell, S. Lin, Z. Tang, H. Häkkinen, N. Zheng, *J. Am. Chem. Soc.* **2015**, 137, 4324-4327.

[16] a) M. S. Bootharaju, C. P. Joshi, M. R. Parida, O. F. Mohammed, O. M. Bakr, *Angew. Chem. Int. Ed.* **2016**, 55, 922-926; b) W. T. Chang, P. Y. Lee, J. H. Liao, K. K. Chakrahari, S. Kahlal, Y. C. Liu, M. H. Chiang, J. Y. Saillard, C. W. Liu, *Angew. Chem. Int. Ed.* **2017**, 56, 10178-10182; c) S. Sharma, K. K. Chakrahari, J. Y. Saillard, C. W. Liu, *Acc. Chem. Res.* **2018**, 51, 2475-2483.

[17] H. G. AbdulHalim, M.S. Bootharaju, Q. Tang, S. D. Gobbo, R. G. AbdulHalim, M. Eddaoudi, D. E.; Jiang, O. M. Bakr, *J. Am. Chem. Soc.* **2015**, 137, 11970-11975.

[18] G. Soldan, M. A. Aljuhani, M. S Bootharaju, L. G. AbdulHalim, M. R. Parida, A. H. Emwas, O. F. Mohammed, O. M. Bakr, *Angew. Chem. Int. Ed.* **2016**, 55, 5749-5753.

[19] Q. Tang, D. E. Jiang, *J. Phys. Chem. C* **2015**, 119, 10804-10810.

[20] T. Chen, S. Yang, J. Chai, Y. Song, J. Fan, B. Rao, H. Sheng, H. Yu, M. Zhu, *Sci. Adv.* **2017**, 3, e1700956.

[21] J. Enkovaara, C. Rostgaard, J. J. Mortensen, J. Chen, M. Dułak, L. Ferrighi, J. Gavnholt, C. Glinsvad, V. Haikola, H. A. Hansen, *J. Phys.*: *Condens. Matter,* **2010**, 22, 253202.

[22] M. Walter, J. Akola, O. Lopez-Acevedo, P. D. Jadzinsky, G. Calero, C. J. Ackerson, R. L. Whetten, H. Grönbeck, H. Häkkinen, *Proc. Natl. Acad. Sci. U.S.A.* **2008**, 105, 9157–9162.

[23] Y. Yu, Q. Yao, K. Cheng, X. Yuan, Z. Luo, J. Xie, *Part. Part. Syst. Charact*. **2014**, 31, 652-656.

[24] a) Q. Li, A. Das, S. Wang, Y. Chen, R. Jin, *Chem. Commun.* **2016**, 52, 14298-14301; b) Y. Chen, C. Liu, H. Abroshan, Z. Li, J. Wang, G. Li, M. Haruta, *J. Catal.* **2016**, 340, 287-294; c) Y. Adachi, H. Kawaasaki, T. Nagata, Y. Obora, *Chem. Lett.* **2016**, 45, 1457-1459.

[25] R. Jin, G. Li, S. Sharma, Y. Li, X. Du, *Chem. Rev*. 2020, DOI: 10.1021/acs.chemrev.0c00495.

10.1002/anie.202011780

WILEY-VCH

COMMUNICATION

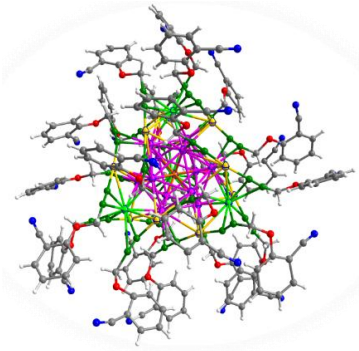

$Au_{13}Ag_{16}$ nanocluster

*Z. Qin, S. Sharma, C.-q. Wan, S. Malola, W.-w. Xu, H. Häkkinen*, and G. Li**

***Page No. 1– Page No.5***

**A Homoleptic Alkynyl-Ligated $[Au_{13}Ag_{16}L_{24}]^{3-}$ Cluster as a Catalytically Active Eight-Electron Superatom**